ELSEVIER

#### Contents lists available at ScienceDirect

# Acta Astronautica

journal homepage: www.elsevier.com/locate/actaastro



# Research Paper

# Modeling and control techniques for landing on (99942) Apophis: An analysis of a mission scenario<sup>☆</sup>

Victor Hernandez Megia a , Tra-Mi Ho , Jan Thimo Grundmann , Matthias Noeker b

- <sup>a</sup> German Aerospace Center (DLR), Institute of Space Systems, Bremen, 28359, Germany
- b German Space Agency at DLR, Bonn, 53227, Germany

#### ARTICLE INFO

# Keywords: Asteroid landing Apophis mission Spacecraft guidance and control Gravitational modeling Sample return missions

#### ABSTRACT

On 13 April 2029, the near-Earth asteroid (99942) Apophis will perform a close flyby within a distance of 32,000 km of Earth's surface. This event, which is ten times closer than the Moon and closer than many geostationary communication satellites, offers an unprecedented opportunity to study an asteroid in great detail. To leverage this close encounter, a fast sample return mission, APOSSUM, was designed using ESA's current RAMSES mission as a use case. This paper presents a detailed analysis of the APOSSUM mission scenario, focusing on feasibility. It covers the separation of the APOSSUM probe, its cruise towards Apophis, and the subsequent landing and return phases. Particular emphasis is placed on the landing scenario, with studies of different density models of Apophis and a comparison of control techniques for precision landing. The findings from this mission will significantly advance our understanding of small-body landing maneuvers.

#### 1. Introduction

Asteroids are essential for understanding the solar system from its emerging stages. They are remnants of the early stages of the solar system and give valuable clues about the basic building blocks that made up a planet or other objects in the solar system. Asteroids are like time capsules, containing information about conditions from 4.5 billion years ago [1]. Most asteroids are located in the Main Belt and the Kuiper Belt.

In the recent past years they have gained significant relevance in the scientific community driven by the information these objects hide in their (sub-) surfaces to understand the building blocks of planets. This information includes not only their composition and formation processes but also potential clues about the origins of life on Earth, as some essential elements for life may have been given by asteroids [2]. This theory is supported by the results of JAXA's Hayabusa2 mission to asteroid Ryugu [3,4] and NASA's OSIRIS-REx to asteroid Bennu [5,6].

Furthermore, studying asteroids can help develop strategies to change their trajectories, thus preventing potential collisions with Earth [7]. The current double mission for planetary defense, DART (Double Asteroid Redirect Test) of NASA [8] and HERA of ESA [9] have these objectives. The DART spacecraft has successfully impacted on Didimorphos, the moonlet of the asteroid binary system Didymos, and was able to change its trajectory setting a step towards a future in which humans are able to deviate asteroids and avoid collisions [10].

In addition to altering the trajectory by a targeted impact, other techniques for asteroid deflection have also been proposed, including the "eccentric collision" approach [11], the directed energy "space ablation" method [12], the "space tug" concept [13], and the "ion beam shepherd" strategy [14]. Each of these methods, while offering advantages for specific scenarios, highlights the breadth of ongoing research dedicated to preventing potential asteroid impacts.

ESA is currently planning a direct successor mission to Hera, the RAMSES mission [15] to be launched in 2028 targeting the near-Earth asteroid (99942) Apophis. This asteroid will encounter Earth in 2029, passing at a distance closer than geostationary orbit at its closest point (= 32,000 km). In this context, the Max Planck Institute for Solar System Research (MPS), together with the German Aerospace Centre (DLR) and the University of Münster, conducted a study on returning asteroid samples from Apophis, the APOphiS SUrfaces saMpler (APOSSUM), using the extremely short return distance to Earth [16]. ESA's RAMSES mission was used in the study as a mission-architectural use case, i.e. the APOSSUM probe should be launched piggybacked with RAMSES as the carrier spacecraft. Thus, all components were adapted to the launcher and to RAMSES to perform the sample recollection and return. In addition to expanding the existing dataset of extraterrestrial materials captured in-situ such as from the Hayabusa, the Hayabusa2 [4] and the OSIRIS-REx missions [6], and thereby increasing our scientific knowledge of asteroids, APOSSUM also aims to

E-mail address: victor.legazpi@gmail.com (V.H. Megia).

https://doi.org/10.1016/j.actaastro.2025.04.031

<sup>\*</sup> Corresponding author.

V.H. Megia et al. Acta Astronautica 235 (2025) 185–194

#### Nomenclature

 $\Delta V$  Change in velocity

AEM Asteroid Exploration Mission APOSSUM APOphiS SUrfaces saMpler AU Astronomical Unit

AU Astronomical Unit
CE Concurrent Engineering

CM Center of Mass

DART Double Asteroid Redirect Test
DLR German Aerospace Center
ESA European Space Agency
FPA Flight Path Angle
G Gravitational Constant

GM Standard Gravitational Parameter
GNC Guidance, Navigation, and Control
HERA ESA Planetary Defense Mission
JAXA Japan Aerospace Exploration Agency

LEO Low Earth Orbit

NASA National Aeronautics and Space Adminis-

tration

NEO Near-Earth Object

PD Proportional-Derivative Control

RAMSES Rapid Apophis Mission for Space Safety

RK45 Runge–Kutta Method (Order 4–5)

SPH Spherical Harmonics SRP Solar Radiation Pressure

STK Systems Tool Kit (Ansys Software)

T Thrust

TC Telecommands

U Gravitational Potential

explore new technological frontiers in spacecraft navigation, guidance and landing techniques [17].

Previous studies have investigated the dynamics and operation of a spacecraft in the proximity of an asteroid [18]. In this article we present different landing scenarios of the APOSSUM probe on Apophis by taking into account two different density scenarios for the asteroid. There are different methods to model the gravitation around an asteroid based on its density distributions. [19] for example employ finite element methods to estimate internal density variations and gravitational fields of small bodies. This study utilizes spherical harmonics and the tetrahedral approach to model Apophis's gravitational potential, specifically to optimize landing maneuvers and develop control techniques tailored to the APOSSUM mission.

### 2. APOSSUM mission overview

The main mission goal of APOSSUM is collecting samples from Apophis' surface and bring them back to Earth. The mission is divided into 3 distinct phases. The first one ("Separation and Approach") deals with the detachment of the APOSSUM probe from the RAMSES spacecraft at a distance of 20 km from Apophis and its flight to the asteroid up to a distance of 1 km. This phase was studied using spherical harmonics and a constant density for the model of Apophis. As will be discussed in further sections, it is a good approximation since the size is insufficient to cause relevant perturbations at those great distances. The results will be presented in the later sections.

The second phase ("landing") covers approaching the asteroid from 1 km above the surface to a target point. For this work, the target point was selected randomly as there is currently no detailed information on the composition of Apophis' surface for dedicated sampling and therefore a random location is used to investigate the control techniques

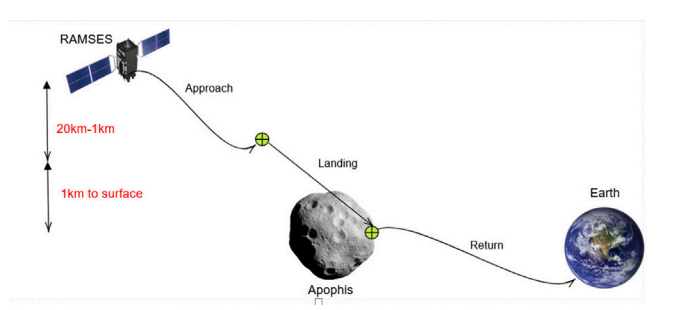


**Fig. 1.** APOSSUM mission scenario. The figure illustrates all three phases as described in the document. Note that it is not to scale and uses a generic asteroid image to represent Apophis.

and scenario. This is in accordance with the mission and scientific requirement of APOSSUM that the landing site should be selected upon arrival. Building upon the orbital dynamic models discussed in [18], our analysis incorporates those perturbations in the landing model but extending them using other shape and density.

As Apophis's density and shape are critical to the final approach phase, as outlined in [20,21], we have analyzed several scenarios to determine the variability of the final approach phase and draw conclusions for navigation during this phase. For this phase, we used Python (specifically using the following libraries :open3d, to open the asteroid model and load the mesh, numpy, for the computations and matplotlib.pyplot, to have a plot style similar to MATLAB [22]) and all the solutions were derived through numerical methods. Different approaches are simulated and compared to provide a detailed assessment of their viability and performance.

Finally, a third phase ("Earth Return") is shown, it involves the return of the APOSSUM lander to a designated landing location on Earth. In this phase, STK is used, assuming an ellipsoid of constant density, since the time it stays in the sphere of influence is short and the main perturbations come from SRP (Solar Radiation Pressure), Lunisolar gravitational effects, and nonsphericity of Earth. The APOSSUM lander will depart from the surface of the asteroid and land in Woomera (Australia), this is the exemplary landing location for this study, similar to the return of the Hayabusa2 samples [4]. The landing location was selected because APOSSUM should land on the opposite side of Earth relative to Apophis during the closest approach. This requirement allows telescopes in other parts of the world to continuously monitor the trajectory of the asteroid and study it during the closest approach.

Fig. 1 illustrates all three phases as described above. Please note that the figure is not to scale. Furthermore, it was created with a generic asteroid image representing Apophis.

#### 3. Model used and its characteristics

Operations at close range, especially when touching or landing on an asteroid's surface depend strongly on the gravity field of the target object. Most dynamic analyses of the approach to an asteroid primarily use spherical harmonics or ellipsoidal harmonics to model the gravity of this small body, as described in the previous section. However, once the operation passes the circumscribing sphere (Brillouin sphere) [19], i.e. in the case of touching the asteroid for sampling, the gravitational field will diverge due to the irregular shape and varying density distribution of the asteroid.

For our analysis of landing maneuvers, we have used the Apophis data obtained by NASA radar observations in 2013 which led to the tetrahedral shape used of the asteroid [23,24], as presented in Fig. 2.

We have chosen this method for modeling the shape of the asteroid, taking into account that there is no case studied in which that amount of vertex and shapes are found to represent Apophis shape. However, V.H. Megia et al. Acta Astronautica 235 (2025) 185–194

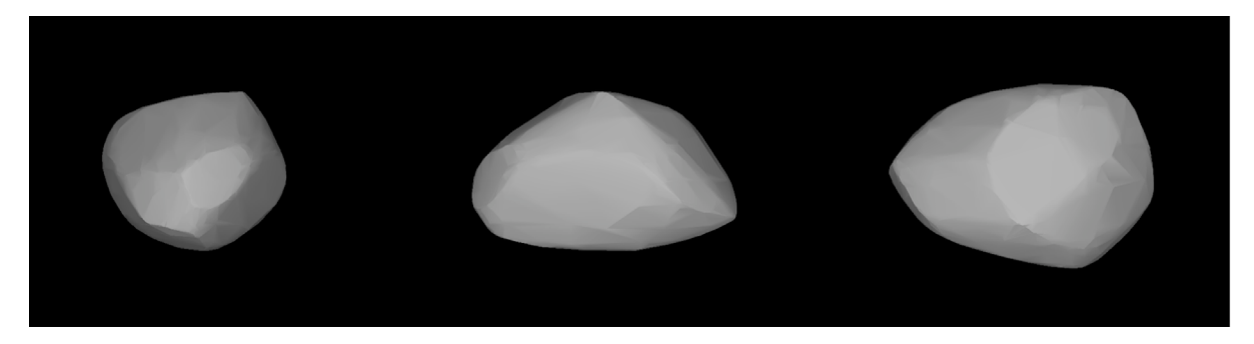


Fig. 2. Apophis shape of the tetrahedral model [23,24].

Table 1
Dimensions of the asteroid Apophis [27].

Variable	Value [m]
x axis	450
y axis	370
z axis	170

this shape model allows us to include different densities and to investigate the dependence of the approach and landing maneuvers of the APOSSUM probe.

The shape model of Apophis [25] was re-constructed using Mesh-Lab, an open-source, purpose-built tool for processing and editing unstructured 3D triangular meshes to enable detailed simulation and analysis [26]. The first step was rescaling the reconstructed model according to the known physical dimensions of Apophis, see Table 1, so the simulations would be in line with real-case scenarios for the APOS-SUM mission. This rescaled mesh serves as the foundational geometric model for further gravitational and landing dynamics simulations. For the bulk density of Apophis, we have adopted for our simulation densities between 1.29 and 3.5 g/cm<sup>3</sup> based on the assessment of [20]. To model the interaction of the APOSSUM probe with the asteroid, we will use different density models. For the "Separation and Approach" phase, we will assume that Apophis has a constant density. For the landing phase, we will model Apophis with varying density distribution since gravitational attraction will diverge within the Brillouin sphere and therefore its influence on the close approach and landing trajectory. Finally, for the return phase, the asteroid will be approximated as a constant density ellipsoid and the main perturbations will come from the lunisolar gravitational attraction, SRP and the non-sphericity of Earth.

The trajectories in this manuscript are generated in an asteroid-fixed coordinate system. This choice allows for accurate modeling of the gravitational field, rotational dynamics, and the relative motion of the lander with respect to Apophis. The asteroid-fixed system is essential for simulations involving trajectory corrections and landing maneuvers, as it captures the local gravitational and rotational effects that influence the spacecraft's approach and stability during touchdown.

#### 4. Phase 1: Separation and approach to apophis

As mentioned in Section 2, the APOSSUM probe will be separated from the RAMSES spacecraft at a 20 km distance. As explained for this phase, we used Spherical Harmonics for trajectory determination and described the gravitational field of Apophis, assuming a bulk density of roughly  $3.2~{\rm g/cm^3}$  which corresponds to a mass of  $6.1 \cdot 10^{10}~{\rm kg}$ . For this first phase and due to the order of magnitude of the distances towards the asteroid, SPH is more suitable because it is more efficient and the detail given by the alternative method used in this study (tetrahedral method) is not needed. Surely, given its size and properties, it is unlikely that Apophis is composed of a single composition, and thus a constant density.

#### 4.1. Spherical harmonics for gravitational field representation

The spherical harmonics are composed of series of orthogonal functions defined on the surface of the sphere to solve problems which involve Laplace's equations in Spherical coordinates. They are used to compute the imperfections of an object and to model it. This approach is convenient from the computational point of view but also from the analytical one since they are able to provide results in a short period of time, while keeping the accuracy in them [28].

$$Y_n^m(\theta,\phi) = \sqrt{\frac{(2n+1)(n-m)!}{4\pi(n+m)!}} P_n^m(\cos\theta) e^{im\phi}$$

Here,  $P_n^m$  are the associated Legendre polynomials, and  $e^{im\phi}$  represents the complex exponential function, essential for incorporating azimuthal symmetry [28].

$$U(r,\theta,\phi) = -\frac{GM}{r} \left( 1 + \sum_{n=1}^{\infty} \left( \frac{R}{r} \right)^n \sum_{m=0}^n P_n^m(\cos \theta) \cdot \left( C_{nm} \cos m\phi + S_{nm} \sin m\phi \right) \right)$$
(1)

where:

- *r* is the radial distance,
- $\theta$  and  $\phi$  are the polar and azimuthal angles, respectively,
- *G* is the gravitational constant,
- *M* is the total mass of the object.
- R is the reference radius of the object which is 185 m [20],
- $C_{nm}$ ,  $S_{nm}$  are the coefficients of the spherical harmonic terms,
- $Y_n^m(\theta, \phi)$  are the spherical harmonic functions

Thus, the real and imaginary coefficients for the harmonic terms are computed as follows:

$$C_{nm} = \sum_{i} \text{Area}_{i} \cdot \text{Re}(Y_{n}^{m}(\theta_{i}, \phi_{i}))$$
 (2)

$$S_{nm} = \sum \operatorname{Area}_{i} \cdot \operatorname{Im}(Y_{n}^{m}(\theta_{i}, \phi_{i}))$$
(3)

Using above formulas applied to the model, the following potentials are obtained.

The resulting potential is nearly constant, and its value is very close to the theoretical one given by  $-\frac{GM}{r}$  [29] as shown in Fig. 3. The resultant mass is  $6.1 \cdot 10^{10}$  kg which corresponds to the density value of 3.2 g/cm<sup>3</sup> (i.e. worst-case scenario, since it is the upper bound of the expected density), both values within the expected range of the asteroid [20]. Additionally, it is noteworthy that the potential is really constant; this is such because the location of the center of mass is shifted just few meters from the origin.

Once the potential is well known, the computation of the trajectory can be obtained. The force is computed knowing that  $F = -\frac{dU}{dr}$  [29]. With that in mind, a dynamic function is created, and using the Runge–Kutta 45 method, the trajectory is computed [30].

To include this influence of SRP, the current designed mass of APOSSUM of approximately 100 kg and the cross-sectional area is

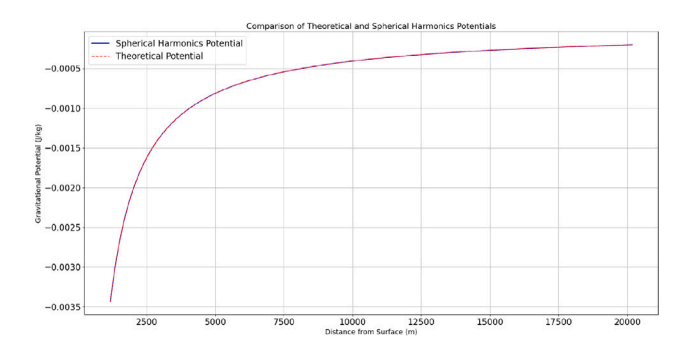


Fig. 3. The calculated potential between 1 km to 20 km distance to Apophis, theoretically and with SPH. The X-axis represents the distance from the surface in meters and the Y-axis the gravitational potential in J/kg

0.2205 m<sup>2</sup> is used as input [17]. In this case, the worst possible scenario was used, and so the spacecraft is always facing the Sun in such a way that the area is maximum.

The SRP formula is computed assuming that the distance from Apophis to the Sun is 1 AU and constant [31]. This is a good approximation since the variation is minimal as shown in [32].

$$\mathbf{a}_{\text{SRP}} = \frac{P_{\text{SRP}} \cdot A_{\text{SRP}}}{m_{\text{sc}}} \mathbf{s} \tag{4}$$

where:

- a<sub>SRP</sub> is the acceleration due to solar radiation pressure,
- $P_{\text{SRP}}$  is the solar radiation pressure at 1 AU (Astronomical Unit) in  $N/m^2$ .
- $A_{SRP}$  is the cross-sectional area of the spacecraft affected by the solar radiation in m<sup>2</sup>,
- $m_{\rm sc}$  is the mass of the spacecraft in kg,
- ${\bf s}$  is the unit vector from the spacecraft towards the Sun, assuming the Sun's influence is along the positive *x*-axis.

In addition, the direction of the pressure was along the x-axis, this is such since it has to be the worst-case scenario and the position of release from RAMSES [15] is still unknown and Apophis is a tumbling rotator. This means that the orientation of the spacecraft with respect to the asteroid and the Sun is not yet defined and the calculations are therefore done to have a conservative result.

With all those factors considered and included in the dynamics function, the trajectory is computed again with the same initial conditions as before. This is shown in Fig. 4

The  $\Delta V$  required to accomplish this maneuver was 1.6 m/s and was achieved over a span of 2.7 h. This  $\Delta V$  can be adjusted to achieve a more fuel-efficient approach by increasing the time required.

Moreover, it can be seen that at these distances and for a first approach, the lander just need one impulse upon arrival and the control technique is still not needed.

#### 5. Phase 2: Landing on Apophis

In this section, the landing maneuvers and scenario will be studied in detail. This phase begins when the APOSSUM spacecraft reaches a distance of 1 km from the surface. A couple of density scenarios are analyzed and ultimately one is selected as the most plausible for the mission.

For this part, we used the tetrahedral method because of the accuracy it brings and the suitability to incorporate several densities in the model. Moreover, according to [33], SPH may produce divergence when computing the trajectories due to the fact that APOSSUM enters the Brillouin sphere.

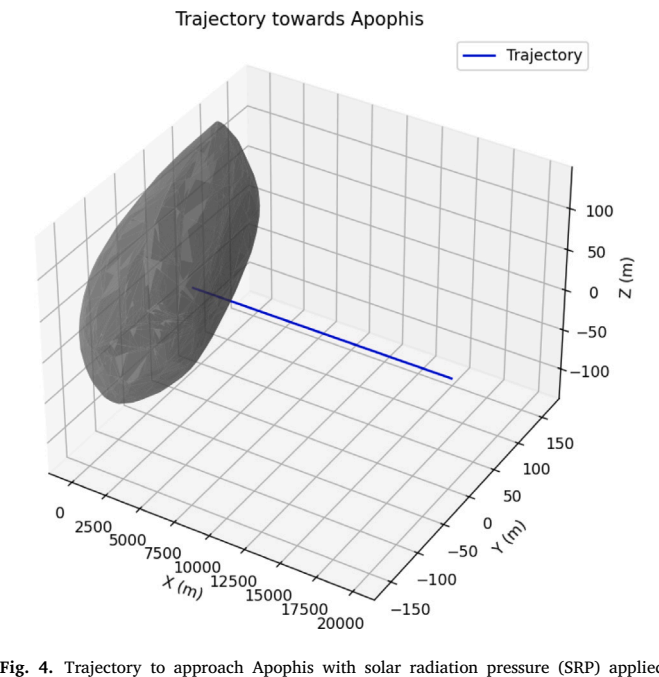


Fig. 4. Trajectory to approach Apophis with solar radiation pressure (SRP) applied. The trajectory showcases the spacecraft's path under the influence of SRP.

#### 5.1. Mesh processing and area calculation

In order to use tetrahedral technique for modeling, the imported mesh of the model is processed to compute key geometric parameters, such as surface area and volume, which are essential for distributing densities accurately across the model.

The model is imported to the code, and the geometric properties of it are computed. These calculations are performed using Heron's formula [34] for all the triangular facets of the mesh, since it is crucial for an accurate distribution of mass over the asteroid's surface.

$$a = \|\mathbf{v}_2 - \mathbf{v}_1\|, \quad b = \|\mathbf{v}_3 - \mathbf{v}_2\|, \quad c = \|\mathbf{v}_1 - \mathbf{v}_3\|$$
 (5)

$$s = \frac{a+b+c}{2} \tag{6}$$

$$Area = \sqrt{s(s-a)(s-b)(s-c)} \tag{7}$$

#### 5.2. Tetrahedral method and gravitational potential

To compute the trajectories in detail, the whole volume of the model is divided in tetrahedral elements [21] using 3 vertices and one middle point chosen to be in the center of the asteroid. The mass is then computed by the formula:

$$m = \rho \cdot V \tag{8}$$

Where V is the volume of the tetrahedral used in that iteration and  $\rho$  the density. The mass is divided in those 3 vertices chosen and the process is repeated for the whole asteroid.

Once the whole mass is computed, the trajectory can be determined. In each step, the gravitational influence of each element is considered. This may not be the most efficient procedure, but it gives accurate results since all elements contribute to the acceleration calculation at every time step. The acceleration exerted by each point mass is given in Eq. (9).

$$\mathbf{a}_{\text{grav}} = -G \sum_{i=1}^{n} \frac{m_i (\mathbf{r} - \mathbf{r}_i)}{|\mathbf{r} - \mathbf{r}_i|^3}$$
(9)

where:

V.H. Megia et al. Acta Astronautica 235 (2025) 185-194

- $\mathbf{a}_{\mathrm{grav}}$  is the total gravitational acceleration exerted on the spacecraft.
- G is the gravitational constant with a value of,  $G = 6.674 \times 10^{-11} \,\mathrm{m}^3 \,\mathrm{kg}^{-1} \,\mathrm{s}^{-2}$ ,
- *n* is the total number of mass elements,
- $m_i$  is the mass of the *i*th tetrahedron element,
- **r** is the position vector of the spacecraft,
- r<sub>i</sub> is the position vector of the center of mass of the ith tetrahedron,
- $|\mathbf{r} \mathbf{r}_i|$  is the distance between the spacecraft and the ith tetrahedron element.

Similarly, to compute the gravitational potential, the value at every point from 1 km above the surface to the surface is computed. This is done using the formula (10)

$$U(\mathbf{r}) = -\sum_{i=1}^{N} \frac{G \cdot m_i}{|\mathbf{r} - \mathbf{r}_i|}$$
 (10)

where

- $U(\mathbf{r})$  is the gravitational potential at the point  $\mathbf{r}$ .
- G is the gravitational constant,  $G = 6.67 \times 10^{-11} \frac{\text{m}^3}{\text{kg s}^2}$
- $m_i$  is the mass of the *i*th tetrahedral element.
- $\mathbf{r}_i$  is the position vector of the center of mass of the ith tetrahedral element.
- $|\mathbf{r} \mathbf{r}_i|$  is the distance between the point of interest  $\mathbf{r}$  and the center of mass of the *i*-the tetrahedral element.

The trajectory of the spacecraft is then simulated by solving the equations of motion, incorporating both the gravitational force and other perturbations such as solar radiation pressure. The motion equation integrated over time is given by Eq. (11).

$$\ddot{\mathbf{r}} = -\nabla U(\mathbf{r}) + \mathbf{a}_{SRP} \tag{11}$$

where:

- $\ddot{\mathbf{r}}$  is the acceleration of the spacecraft,
- $U(\mathbf{r})$  is the gravitational potential at the position  $\vec{r}$  of the space-
- $\mathbf{a}_{\text{SRP}}$  is the acceleration due to solar radiation pressure acting on the spacecraft.

This detailed accounting ensures precise modeling of the space-craft's trajectory as it moves through the asteroid's gravitational field, considering both the micro-variations in the asteroid's density and macro-level influences such as solar radiation. Thus, the trajectories are computed. With the computed trajectories established, we proceed to analyze non-constant density scenarios.

#### 5.3. Non-constant density scenarios

Most smaller asteroids are thought to be rubble piles, i.e. debris of different sizes and shapes that have coalesced under the influence of gravity. In the case of Itokawa, [35], an S-type Near-Earth asteroid visited by the Hayabusa mission (JAXA), the asteroid is divided into a higher and lower density lobe. Thus, we have adapted this case to model Apophis, e.g. assuming that the asteroid is divided into two different density regions, see Fig. 5. We have chosen 3.2 g/cm $^3$  and 1.29 g/cm $^3$  as density values, which are roughly the upper and lower limits for Apophis.

The associated trajectories around Apophis with a 2-density distribution are shown in Fig. 6. For this 2-density distribution, we obtained a total mass of the asteroid of approx.  $4.5 \cdot 10^{10}$  kg which is within the expected limits defined by [20]. The trajectory of the APOSSUM probe towards Apophis is almost circular, as seen in Fig. 6, however the path is slightly perturbed due to the influence of the SRP.

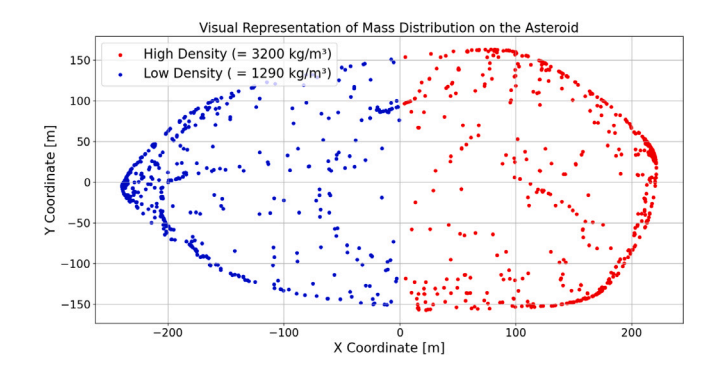
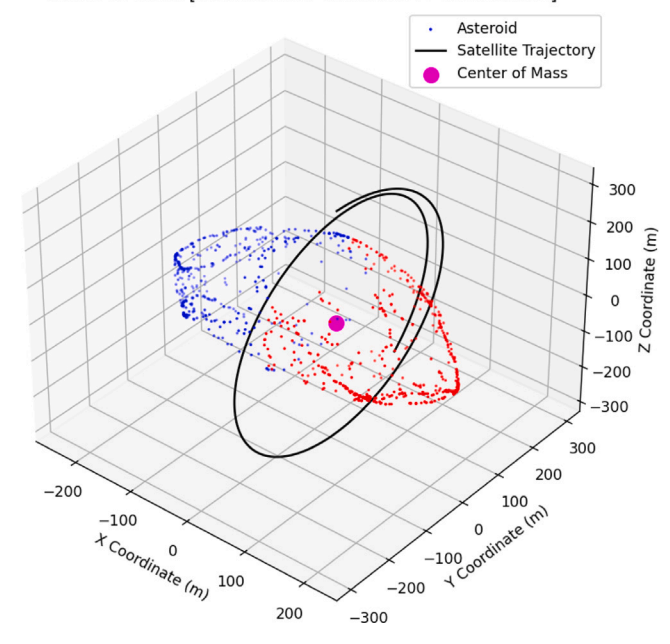
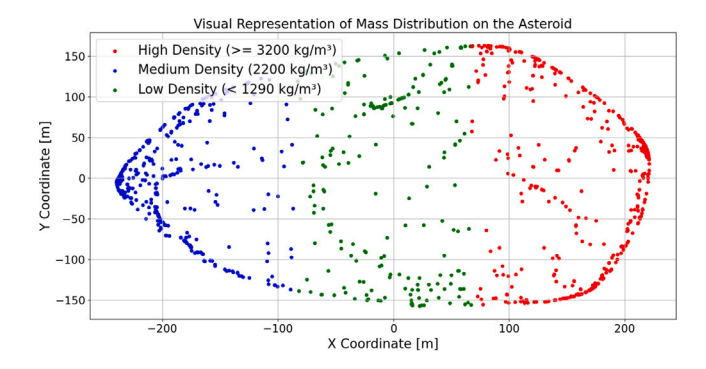


Fig. 5. Apophis modeled using the tetrahedral method with 2-density distribution. The blue region represents a density of  $1.29 \text{ g/cm}^3$ , while the red region corresponds to  $3.2 \text{ g/cm}^3$ . (For interpretation of the references to color in this figure legend, the reader is referred to the web version of this article.)

Total Mass of Asteroid: 45597741123.75 kg Center of Mass: [37.19237071 -0.28546244 0.90080971]



 $\textbf{Fig. 6.} \ \ \text{Trajectory simulation around Apophis using the tetrahedral method with two density lobes.}$ 



**Fig. 7.** Apophis with three density lobes modeled using the tetrahedral method. The blue region represents a density of  $1.29~\rm g/cm^3$ , the green region  $2.2~\rm g/cm^3$ , and the red region  $3.2~\rm g/cm^3$ . (For interpretation of the references to color in this figure legend, the reader is referred to the web version of this article.)

Total Mass of Asteroid: 42322840004.22 kg Center of Mass: [ 1.74976610e+01 2.74245644e-03 -2.78797352e+00]

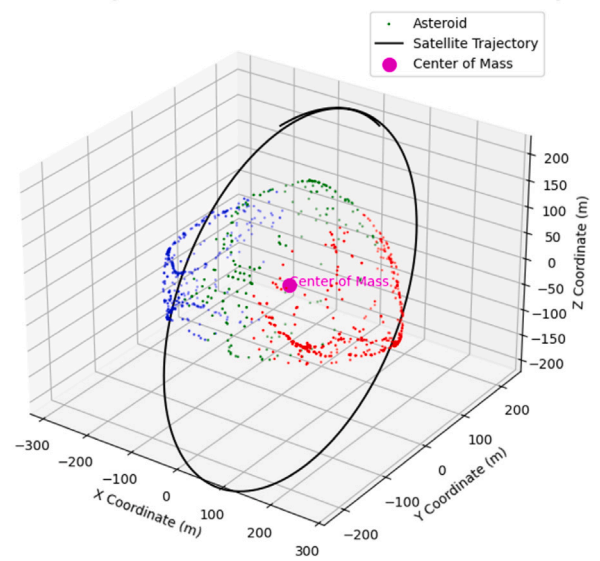


**Fig. 8.** Trajectory path of the APOSSUM lander for the 3-density distribution case of Apophis. The path is influenced by high-density lobes and central mass attraction, showcasing adjustments from gravitational perturbations and solar radiation pressure.

In addition, we also looked into a 3-density distribution case for Apophis assuming 3 lobes with respective densities:  $3.2 \, / \, \mathrm{cm}^3$ ,  $2.2 \, / \, \mathrm{cm}^3$  and  $1.29 \, \, \mathrm{g/cm}^3$ . The three lobe density distribution is shown in Fig. 7. As illustrated in Fig. 8, the trajectory is perturbed in such a way that it tends to align towards the center of mass while being influenced simultaneously by the gravitational attraction of the denser lobe. The initial velocity used corresponds to the theoretical one using the mass of the asteroid, calculated using  $\sqrt{\frac{GM}{r}}$  [36]. Although the trajectory is close to circular, it is not exact, as for the 2 density-lobe scenario. This is because, in this scenario, the gravitational perturbation is more complex, and the SRP is also taken into account, as explained in the previous study case.

As explained, the two density scenarios reveal significant differences in the behavior of APOSSUM's trajectory and the position of the center of mass due to the density scenarios. For the 2-density asteroid case the center of mass has a greater shift towards the denser lobe than for the 3-density asteroid scenario. In addition, the orbital period of the spacecraft varies between the two cases, as it depends on the mass of the asteroid. As shown in the figures, the APOSSUM probe is able to make almost 1.5 rotations in the 2-density lobe scenario and barely one in the other case. This discrepancy is attributed to the initial velocity used, which is proportional to the mass of the asteroid. Since the mass is higher in the first case, the resulting velocity is also higher, leading to a shorter rotation period.

This observation indicates that upon arrival, depending on the actual density distribution of Apophis, a more thorough investigation of the asteroid's density will be required to determine the most reliable landing trajectory for the APOSSUM probe.

#### 5.4. Controlled landing on Apophis

Once the non-uniform density scenario has been established, control techniques can be applied for landing. Usually, the most efficient maneuver would be computed by trial and error to use the gravitational potential in favor of the spacecraft and so orbit it as it lands in a curved trajectory. Since the APOSSUM probe has to communicate with RAMSES [15], we have to anticipate a rectilinear trajectory for APOSSUM and therefore we have to look for an optimized control technique.

Table 2
Best trial using PD control with updated gains.

Кр	Kd	Δt [s]	$\Delta V$	Tol.	Time [s]	Success
0.005	0.002	12.5 & 1	2.63	2	1635	Success

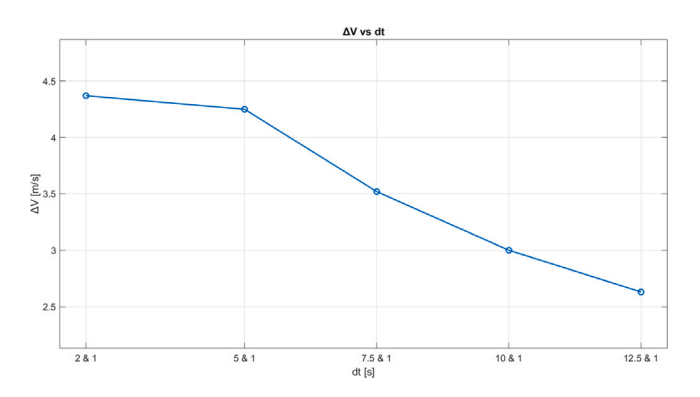


**Fig. 9.** Results using PD control to reduce the time step. The plot compares the total  $\Delta V$  against the time step between corrections.

To achieve a successful landing, 2 control techniques have been tested, including the proportional derivative control (PD) [37] and the Bang-Bang control [38].

In PD control, the control input is based on both the current error and the rate of change of the error (which is the derivative term). It calculates the desired velocity change using a proportional term and the current velocity, which acts as a derivative term [39].

$$\Delta \mathbf{V} = K_p \, \mathbf{e}(t) + K_d \, \frac{d\mathbf{e}(t)}{dt} \tag{12}$$

where:

- $\Delta V$  is the vector increment of velocity (the control output).
- $K_p$  is the proportional gain.
- $\mathbf{e}(t)$  is the error vector (difference between the target position and the current position).
- $K_d$  is the derivative gain.
- $\frac{de(t)}{dt}$  is the rate of change of the error (difference between the target velocity and the current velocity).

Moreover, it has to be mentioned that for these calculations a maximum  $\Delta V$  and a minimum one were set. These values were computed using Newton's equation and the corresponding thrust of the engine used in the spacecraft.

$$\Delta V = \frac{T \cdot \Delta t}{m_{sc}} \tag{13}$$

Several trials were conducted to fine-tune the parameters and optimize the results in every iteration.

As shown in Table 2, using PD control method, the required time for the spacecraft to land is 1635 s and the  $\Delta V$  is relatively low. This low value is achieved by doing small increments in velocity along the path, and therefore the needed time rises. Moreover, Fig. 9 is shown to have a deeper view of the relationship between the minimum time step at which the algorithm corrects the trajectory, and the  $\Delta V$ . The 2 values on each position on the x-axis are due to the fact that this technique uses 2 different minimum time step corrections along the path. When the lander is at a height greater than 50 meters the  $\Delta t$  used is the greater value, in this case varies for every trial from 12.5 to 2 s, whereas for closer distances, it is reduced to 1 s. For APOSSUM, this altitude of 50 meters was selected as the transition point to fine control, aligning with Hayabusa2's successful sampling strategy. It provides sufficient time to mitigate gravitational perturbations and ensure a stable touch-and-go operation [40].

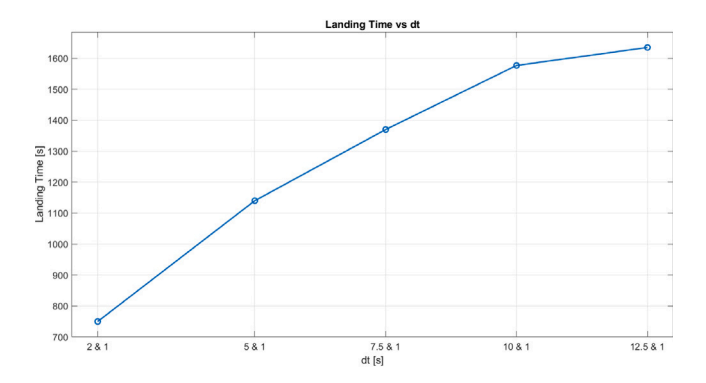


**Fig. 10.** Results using PD control to reduce the time step. The *Y*-axis shows the landing time in seconds, while the *X*-axis shows the time step in seconds.

Table 3
Best trial using Bang-Bang control.

Кр	$\Delta t$	$\Delta V$	Tol.	Time [s]	Success
-	1	3.94	3	458	Success

Additionally, Fig. 9 shows a linear trend where a reduction in time step results in a smaller  $\Delta V$ . This allows APOSSUM to save more propellant on the way at a time cost, as it can be seen in Fig. 10.

On the other hand, Bang-Bang control technique is a simple on-off control strategy where the control input is switched between its maximum and minimum values of thrust to drive the system towards a desired state. This control technique is often used in the case precise control is not required, and the system can tolerate abrupt changes [41].

$$\mathbf{e}(t) = \mathbf{r}_{\text{target}} - \mathbf{r}(t). \tag{14}$$

Where  $\mathbf{r}_{\text{target}}$  is the target location and  $\mathbf{r}(t)$  is the actual position at time t of the lander.

The unit error vector is obtained by normalizing the error vector to get the direction in which the spacecraft needs to move.

$$\Delta V = \begin{cases} \Delta V_{\text{max}} & \text{if } \mathbf{e}(t) \ge 0\\ -\Delta V_{\text{max}} & \text{if } \mathbf{e}(t) < 0 \end{cases}$$
 (15)

This correctly shows that the change in velocity  $\Delta V$  is set to  $\Delta V_{max}$  (which is the one corresponding to the maximum thrust) if the error vector (e(t)) is positive, and  $-\Delta V_{max}$  if the error vector is negative. Moreover, one may have noticed the maximum  $\Delta V$  is the same as for the PD control technique.

The rotation of the asteroid was also taken into account for these studies. The period used was 30.56 h, as shown in [42,43].

When comparing these techniques, both have merits to be suitable; nevertheless, one of them is better for landing than the other.

Although the Bang-Bang control algorithm is relatively straightforward to implement and achieves an earlier arrival at the landing site, its reliance on high-thrust impulses results in significantly higher fuel consumption, as shown in 3. On the other hand, Table 3 shows that the landing time is significantly reduced when using Bang-Bang. This is due to the switch between maximum thrust and none. Although this approach reduces time, it does so by increasing the propellant usage. So, it can be noticed that this is a suitable option in case there is a strict time constraint. Nevertheless, since APOSSUM is not driven by a time constraint, it is preferred to save propellant for the return from the asteroid to Earth. Moreover, it is worth mentioning that more trials have been done using Bang-Bang, and for tolerances smaller than 2.7 m, it fails to land within that tolerance, and further tuning may be needed.

Fig. 11 shows the trajectory of the APOSSUM probe to a target location on the surface of the asteroid. The  $\Delta V$  is 2.63 m/s as shown in Table 2, the resulting path is almost rectilinear. Furthermore, landing velocity meets the requirements of the GNC subsystem, which specifies

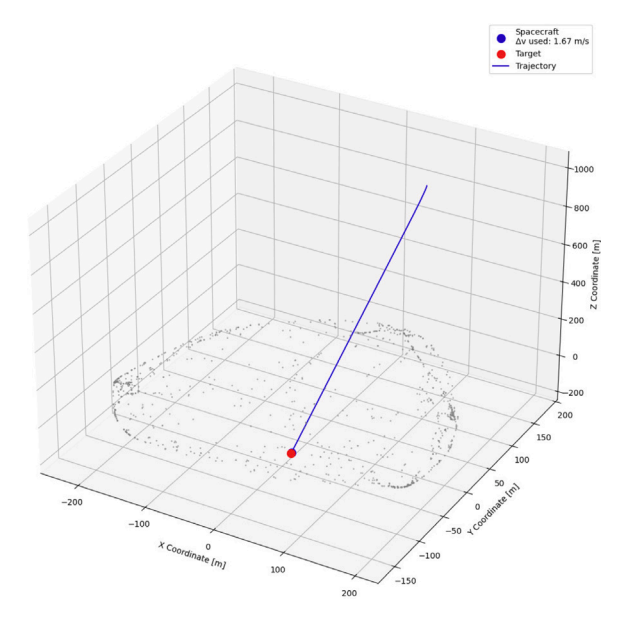


Fig. 11. Final trajectory using PD control to land.

Table 4
Comparison of 2-lobe vs. 3-lobe distributions using the PD controller.

Model	V. Vel.	L. Vel	Time [s]	$\Delta V$	Success
2-lobe	-0.082	0.057	1327	3.15	No
3-lobe	-0.093	0.036	1635	2.63	Yes

a maximum vertical velocity of  $0.2\,\mathrm{m/s}$  and a maximum lateral velocity of  $0.05\,\mathrm{m/s}$  to prevent rebound. The spacecraft successfully landed with a vertical velocity of  $0.09\,\mathrm{m/s}$  and a lateral velocity of  $0.05\,\mathrm{m/s}$ . The reason behind these requirements comes from the experience of Osiris-Rex [44] and Hayabusa2 [45], the restrictions of the vertical and lateral velocity have been defined during the design process to be  $0.2\,\mathrm{m/s}$  and  $0.05\,\mathrm{m/s}$  respectively, very similar to the values used in those missions. This will allow a spring-loaded touchdown of APOSSUM and guarantees that the sampler will not tilt.

## 5.5. Limitations of the PD control

Once the PD control technique was chosen based on its suitability for the mission, it became necessary to verify whether this controller can handle a variety of density distributions and conditions. Although the PD controller performs adequately in the three-lobe scenario described above, its limitations need to be accounted for in case this method is not suitable for all configurations.

For the identification of potential limitations, the alternative model from Section 5.3 is considered, which describes the 2 density-lobe scenario. That model provides another internal structure of the asteroid, and hence presents another possible environment of the APOSSUM upon arrival. Using the same PD gains and  $\Delta V$  limits as before, is expected to identify whether the controller would fail the final velocity constraints or needs further adaptation.

Please note that the velocities of Table 4, are in m/s. As it can be seen, the controller meets the vertical and lateral velocity requirements only in the three-lobe scenario. In the two-lobe case, the larger lateral offset induces a final lateral velocity slightly above  $0.05\,\mathrm{m/s}$ , thus failing the requirement. These findings indicate that while the PD controller is successful for the three-lobe model, it may require fine-tuning for other density distributions. The next subsection extends these analyses via a Monte Carlo simulation (Section 5.6), focusing primarily on the three-lobe scenario.

Table 5
Monte Carlo simulation parameters.

Parameter	Variation	Distribution
Mass (kg)	Uniform	100 ± 10
Area (m²)	Uniform	$0.22 \pm 0.05$
Position Noise (m)	Gaussian	$\mu = 0, \ \sigma = 0.1$
Velocity Noise (m/s)	Gaussian	$\mu = 0, \ \sigma = 0.01$
Gravitational Model Error (%)	Gaussian	$\mu = 0\%, \ \sigma = 5\%$
SRP Force Noise (%)	Gaussian	$\mu = 0\%, \ \sigma = 2\%$
Density High (kg/m³)	Uniform	$3200 \pm 300$
Density Mid (kg/m³)	Uniform	$2200 \pm 200$
Density Low (kg/m³)	Uniform	$1290 \pm 100$

#### 5.6. Monte Carlo simulation

In order to assess the reliability and accuracy of the modeled landing maneuver with the parameters used in the PD control technique and to provide a quantified success rate, a Monte Carlo simulation was performed taking into account relevant uncertainties.

As summarized in Table 5, the parameters that were varied in the Monte Carlo simulation are relevant variables of the system. The mass and cross-sectional area of APOSSUM were varied by 10% and 22%, respectively, to account for any possible future change. Moreover, some position and velocity noises were introduced using Gaussian distributions to simulate sensor inaccuracies. In addition, the simulation also tries to take into account the gravitational model error and the SRP force noise for those cases in which some errors in the measurement are made, and the gravitational perturbations from 3rd bodies like Earth, although the influence of these is negligible for the chosen mission scenario due to the large distance. Finally, the 3 density values were changed in a uniform way to represent material inconsistencies within Apophis.

Using those parameters, a Monte Carlo simulation was done for 5000 cases and APOSSUM achieved a 99.96% success. For a case to be successful, it has to land within the 3 meter location threshold, its terminal velocity has to be below the escape velocity, and it has to fulfill the requirements of the vertical and lateral maximum velocities.

The average terminal velocity error was found to be 0.10~m/s, with the maximum terminal velocity error also recorded at 0.10~m/s, demonstrating consistent and minimal velocity deviations across all simulations. The Average Position Error was 0.99~m, which is well within the predefined distance tolerance limits, further confirming the precision and reliability of the PD controller with timestep variation at 50~m altitude under varied operational conditions.

#### 6. Phase 3: Return to Earth

Once the samples are collected, the sample phase ends and so the return to Earth begins.

The landing location on Earth is chosen to be Woomera, the exemplary landing location for this study, which is the dessert part of Australia (-31°,128°). This location is selected because of its sparse population, which minimizes the risk to human life and property. Moreover, the mission design also considers that the asteroid needed to be on the opposite side of the Earth during the landing in Woomera to ensure undisturbed observation of Apophis by the telescopes. For the departure date from Apophis several dates were considered as candidates, and so several simulations were computed in order to see the best fit.

As shown in Figs. 12 and 13, the closer the departure date is to the closest encounter of Apophis to Earth, the more  $\Delta V$  is needed for the return. This is because the trajectory needs a greater correction and acceleration to arrive on the same date. A tradeoff was made, taking this fact into account along with the requirement of the FPA (Flight Path Angle) that the APOSSUM probe must have when approaching LEO (20° or less) for reentry into the atmosphere [46].

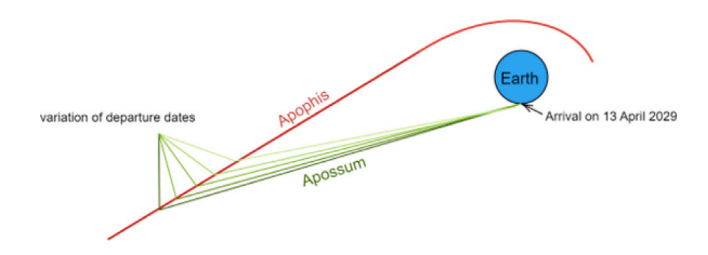


Fig. 12. Returning dates.

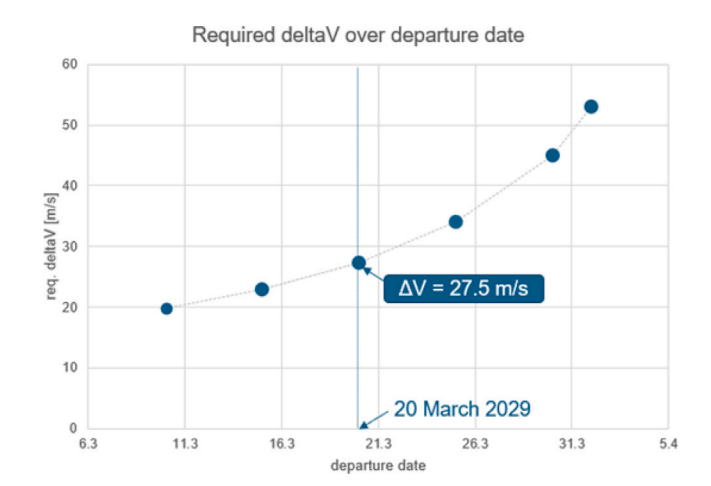


Fig. 13.  $\Delta V$  associated with the respective departure dates.

Taking these data and requirements into consideration, the departure date was chosen to be 20 March 2029 and the resulting day of arrival on Earth is 13 April 2029, which corresponds to the closest distance of Apophis to Earth [47].

# 7. Summary and conclusion

This paper presents a study of the mission scenario of an asteroid sample return mission, APOSSUM, to the asteroid Apophis using ESA's RAMSES spacecraft as a carrier. The presented work particularly focused on the controlled landing of the APOSSUM probe assuming that Apophis bulk density is not constant. In contrast to the findings of [18], it provides insight into control strategies that can be used to counteract the perturbations that the spacecraft may encounter during the landing phase in a complex density scenario.

The incorporation of a non-constant density model represents a significant departure from traditional landing analyses, which often assume a uniform density distribution. In the case of target asteroids such as Ryugu (Hayabusa2) and Bennu (Osiris-Rex), which exhibit high density homogeneity and shape symmetry, the latter approach is applicable for landing planning by determining the gravity field over multiple approach or hover maneuvers. In the case of an asymmetric asteroid such as Itokawa or (probably) Apophis, possible higher density inhomogeneities, which can strongly influence the landing maneuver, must be considered during the landing approach. Especially for mission concepts with a short duration, such as APOSSUM on RAMSES or other mission concepts [48-50], which require a short deployment time on the asteroid, an adaptive control design is required to optimize the long-term hovering flight and the analysis of the gravitational field. The introduction of dynamic time steps during trajectory corrections or the refinement of control gains based on local gravity gradients could further improve landing precision and fuel efficiency. These results provide valuable information for landing missions targeting asteroids with complex internal structures to develop more robust guidance and control systems.

V.H. Megia et al. Acta Astronautica 235 (2025) 185–194

The Key Findings in terms of **Control techniques**: Phase 1, the "Separation and Approach", can be carried out without any control technique using one impulse. For Phase 2, the PD control technique has proved to be a better option for landing, as there is no strict time restriction and thus saving  $\Delta V$  is preferred [51]. Moreover, the trajectory of the Bang-Bang approach will be less stable and straight due to the explained changes between maximum and zero thrust [38]. This means that for a mission with a stronger restriction in time, rather than fuel consumption and robustness (not being able to land within a tolerance smaller than 2.7 m), a Bang-Bang control strategy is a more suitable option.

Furthermore, while the PD control method proved highly effective for the APOSSUM mission scenario, it is not without limitations. The need for precise time step tuning and reliance on accurate gravitational models could pose challenges for real-time adaptability to other asteroids. Additionally, it requires computational resources for adaptive time steps and potential overcorrection risks during final descent highlight areas for future optimization. These limitations point to the potential benefits of integrating more advanced control strategies, such as model-predictive control or hybrid approaches, to further enhance robustness and efficiency.

Landing Precision The precision is higher with a PD control as it enables modular thrust, which is a great advantage when trying to land in a small landing place. This is crucial for missions requiring exact placement of the spacecraft, particularly in regions with challenging topography or when specific scientific objectives require landing tolerances under 2.7 m. In contrast, Bang-Bang control may not achieve such high precision without significant additional tuning, making it less reliable for tight landing requirements.

The use of PD and Bang-Bang control for a mission with changing density distributions revealed both limitations and areas for improvement. Without adjustments like varying time steps in PD control, the lander would struggle to achieve precise landings within a 3-meter radius, as gravitational perturbations near denser lobes significantly affect trajectory stability. Bang-Bang control, while faster, consumes more fuel due to its reliance on high-thrust impulses, making it less efficient for fuel-limited missions. Moreover, this control technique needs fine-tuning and is not recommended for these kinds of missions.

Future missions could benefit from implementing dynamic time steps during trajectory corrections or fine-tuning control gains. These adjustments would allow spacecraft to better handle irregular gravitational environments and improve landing precision, particularly in missions targeting small or highly variable landing areas. Such strategies would improve robustness and minimize fuel consumption under challenging conditions.

Impact of Density Variations: The study also explored the impact of Apophis's density variations on the spacecraft's trajectory. Changing density distributions were found to cause significant perturbations in the trajectory, which makes it essential to account for these variations in control techniques to ensure a successful landing. The finally selected density distribution is an example that corresponds to the case of a 3-density lobe distribution.

In conclusion, this research provides information on the control techniques to land on an asteroid, showing different scenarios and control techniques for a successful mission. The findings are helpful for future mission campaigns that want to explore small celestial bodies, since a similar approach can be used from the guidance, navigation, and control perspective. The same framework can be utilized for other mission objectives, even when the targets are located farther away but remain within a few lunar distances from Earth. For instance, those aiming to land on near-Earth objects (NEOs) or even conduct sample return operations from distant asteroids. For these cases, the approach can be similar by adapting the densities and shape to correspond to the target asteroid. The only significant difference would be in the return phase, as this spacecraft is designed to account for the close proximity of Apophis during its encounter. Other targets may require more time and a higher  $\Delta V$ .

#### CRediT authorship contribution statement

Victor Hernandez Megia: Writing – original draft, Visualization, Software, Methodology, Investigation, Formal analysis. Tra-Mi Ho: Writing – review & editing, Validation, Supervision, Project administration, Methodology, Investigation, Conceptualization. Jan Thimo Grundmann: Writing – review & editing, Investigation. Matthias Noeker: Writing – review & editing.

#### Declaration of competing interest

The authors declare that they have no known competing financial interests or personal relationships that could have appeared to influence the work reported in this paper.

#### References

- C. Wolner, 1. a time capsule from the early solar system is en route to earth, Eos (2022) http://dx.doi.org/10.1029/2022eo220370.
- [2] E. Anders, Pre-biotic organic matter from comets and asteroids, Nature 342 (1989) 255–257, http://dx.doi.org/10.1038/342255a0.
- [3] H. Yabuta, G.D. Cody, C. Engrand, Y. Kebukawa, Macromolecular organic matter in samples of the asteroid (162173) Ryugu, Science 379 (6634) (2023) eabn9057, http://dx.doi.org/10.1126/science.abn9057, arXiv:https://www.science.org/doi/ pdf/10.1126/science.abn9057.
- [4] Y. Oba, Y. Takano, J.P. Dworkin, Ryugu asteroid sample return provides a natural laboratory for primordial chemical evolution, Nature 14 (2023) http://dx.doi.org/10.1038/s41467-023-38518-1, URL https://www.nature.com/ articles/s41467-023-38518-1.
- [5] D.S. Lauretta, H.C. Connolly, J.E. Aebersold, C.M.O. Alexander, R.L. Ballouz, Asteroid (101955) bennu in the laboratory: Properties of the sample collected by OSIRIS-REx, Meteorit. Planet. Sci. 59 (9) (2024) 2453–2486, http://dx.doi. org/10.1111/maps.14227.
- [6] D.S. Lauretta, H.C.C. Jr, J.E. Aebersold, Asteroid (101955) Bennu in the laboratory: Properties of the sample collected by OSIRIS-REx, Meteorit. Planet. Sci. 59 (9) (2024) 2453–2486, http://dx.doi.org/10.1111/maps.14227, URL DOI: 10.1111/maps.14227.
- [7] B.D. Seery, M. Bambacus, R. Leung, K. Greenaugh, F. Raccah, M. Boslough, C. Yang, Near earth object mitigation studies, in: 2016 IEEE Aerospace Conference, IEEE, 2016, pp. 1–12, http://dx.doi.org/10.1109/AERO.2016.7500546.
- [8] M.E. Banks, DART mission deflects asteroid in first-of-its-kind test, Phys. World 35 (11) (2022) 13i, http://dx.doi.org/10.1088/2058-7058/35/11/16.
- [9] P. Michel, M. Kueppers, I. Carnelli, H.S. Team, The ESA hera mission to the near-earth asteroid binary (65803) didymos: Documentation of the NASA dart impact and full characterization of the asteroid system, Bull. the AAS 55 (8) (2023) http://dx.doi.org/10.3847/25c2cfeb8a0a2400012fa45f, URL https://baas. aas.org/pub/2023n8i201p07.
- [10] A. Buscarino, C. Famoso, L. Fortuna, G.L. Spina, NASA dart mission: A preliminary mathematical dynamical model and its nonlinear circuit emulation, Nonlinear Eng. 12 (1) (2023) 20220314, http://dx.doi.org/10.1515/nleng-2022-0314.
- [11] K. Lee, Z. Fang, Z. Wang, Investigation of the incremental benefits of eccentric collisions in kinetic deflection of potentially hazardous asteroids, Icarus 425 (2025) 116312, http://dx.doi.org/10.1016/j.icarus.2024.116312.
- [12] P. Lubin, G. Hughes, J. Bible, Directed energy planetary defense, Opt. Eng., Bellingham 53 (2) (2014) 025103, http://dx.doi.org/10.1117/1.OE.53.2.025103.
- [13] J.P. Sánchez, et al., Multicriteria comparison among several mitigation strategies for dangerous near-earth objects, J. Guid. Control Dyn. 32 (1) (2009) 121–142, http://dx.doi.org/10.2514/1.35588.
- [14] C. Bombardelli, J. Pelaez, The ion beam shepherd: A new concept for asteroid deflection, Acta Astronaut. 90 (1) (2013) 98–102, http://dx.doi.org/10.1016/j. actaastro.2012.07.008.
- [15] ESA, Introducing ramses, esa's mission to asteroid apophis, 2024, https://www.esa.int/Space\_Safety/Planetary\_Defence/Introducing\_Ramses\_ESA\_s\_ mission\_to\_asteroid\_Apophis.
- [16] M. Hilchenbach, O.J. Stenzel, C. Renggli, A. Nathues, N. Krupp, H. Fischer, T. Kleine, J. Biele, S. Ulamec, J.T. Grundmann, T.-M. Ho, C. Güttler, B. Gundlach, M. Goldmann, N. Schmitz, N. Aksteiner, S. Chand, F. Eichstaedt, O. Eßmann, H. Feiler, T. Firchau, S. Fexer, P. Goldyn, M. Heberhold, V. Hernandez Megia, E. Ksenik, M. Lange, P. Marquardt, F.C. Passenberg, D. Quantius, A. Schneider, F.M. Seibert, M. Siemer, S. Theil, G. Tsakyridis, N. Wendel, T. Wippermann, L. Witte, Snatching a probe of a genuine near-earth asteroid: Fast sample return opportunity in the frame of RAMSES mission scenario, in: Apophis T-5 Years Workshop, in: Apophis T-5 Years, (#2011) USRA, 2024.

- [17] T.M. Ho, M. Hilchenbach, J.T. Grundmann, S. Ulamec, J. Biele, F. Dannemann, B. Gundlach, H. Fischer, C. Gittler, M. Grott, T. Kleine, N. Krupp, M. Lange, A. Nathues, D. Quantius, Scientifically strengthening an asteroid mission with small probes on RAMSES as use case, in: Proceedings of the International Astronautical Congress, IAC, in: IAC-24, A3, 4A, 10, x85066, International Astronautical Congress (IAC), Milan, Italy, 2024.
- [18] D. Scheeres, Proximity operations about apophis through its 2029 earth flyby, 2022, http://dx.doi.org/10.48550/arXiv.2211.10903, Available at: https://arxiv. org/abs/2211.10903.
- [19] R.S. Park, R.A. Werner, S. Bhaskaran, Estimating small-body gravity field from shape model and navigation data, J. Guid. Control Dyn. 33 (1) (2010) 212–221, http://dx.doi.org/10.2514/1.41585.
- [20] G. Valvano, O.C. Winter, R. Sfair, R. Machado Oliveira, G. Borderes-Motta, T.S. Moura, APOPHIS – effects of the 2029 Earth's encounter on the surface and nearby dynamics, Mon. Not. R. Astron. Soc. 510 (1) (2021) 95–109, http://dx.doi.org/10.1093/mnras/stab3299.
- [21] Y. Weidong, L. Shu, Y. Yu, Y. Gao, Use of tetrahedral finite element method for computing the gravitation of irregular-shaped asteroid, IOP Conf. Ser.: Mater. Sci. Eng. 608 (2019) 012043, http://dx.doi.org/10.1088/1757-899X/608/1/012043.
- [22] MathWorks, MATLAB the language of technical computing, 2024, URL https://de.mathworks.com/products/matlab.html. (Accessed 26 November 2024).
- [23] L.-L. Yu, J. Ji, W.-H. Ip, Surface thermophysical properties investigation of the potentially hazardous asteroid (99942) apophis, Res. Astron. Astrophys. 17 (2017) http://dx.doi.org/10.1088/1674-4527/17/7/70.
- [24] P. Pravec, P. Scheirich, J. Ďurech, J. Pollock, P. Kušnirák, The tumbling spin state of (99942) apophis, Icarus 233 (2014) 48–60, http://dx.doi.org/10.1016/ j.icarus.2014.01.026.
- [25] G. Frieger, Asteroid (99942) apophis 3D model, 2021, URL https://3d-asteroids. space/asteroids/99942-Apophis. (Accessed: 02 December 2024).
- [26] MeshLab, MeshLab, 2024, URL https://www.meshlab.net/. (Accessed: 02 December 2024).
- [27] M. Brozović, L.A.M. Benner, J.G. McMichael, J.D. Giorgini, P. Pravec, P. Scheirich, C. Magri, M.W. Busch, J.S. Jao, C.G. Lee, L.G. Snedeker, M.A. Silva, M.A. Slade, B. Semenov, M.C. Nolan, P.A. Taylor, E.S. Howell, K.J. Lawrence, Goldstone and arecibo radar observations of (99942) apophis in 2012–2013, Icarus 300 (2018) 115–128, http://dx.doi.org/10.1016/j.icarus.2017.08.032.
- [28] S. Goossens, D.E. Smith, Gravity degree–depth relationship using point mass spherical harmonics, Geophys. J. Int. 233 (3) (2023) 1878–1889, http://dx.doi. org/10.1093/gji/ggad036.
- [29] J.R. Taylor, Classical Mechanics, University Science Books, Sausalito, CA, 2005.
- [30] S.J. Mohammed, M.A. Mohammed, Runge-kutta numerical method for solving nonlinear influenza model, 2021, http://dx.doi.org/10.1088/1742-6596/1879/ 3/032040.
- [31] D.A. Vallado, Fundamentals of astrodynamics and applications, in: 4th ICATT, Madrid, Spain, Tutorial Lectures, European Space Agency (ESA), 2010, URL https://trajectory.estec.esa.int/Astro/4rth-astro-workshop-presentations/ICATT-2010-Tutorial-ASTRODYNAMICS.pdf.
- [32] V. Pesce, A. Colagrossi, S. Silvestrini, Modern Spacecraft Guidance, Navigation, and Control, Elsevier, 2023, http://dx.doi.org/10.1016/C2020-0-03563-2.
- [33] Y. Takahasi, Spherical harmonic potentials within the brillouin sphere, in: AIAA/AAS Astrodynamics Specialist Conference, American Institute of Aeronautics and Astronautics (AIAA), 2014, http://dx.doi.org/10.2514/6.2014-4202
- [34] K.F. Riley, M.P. Hobson, S.J. Bence, Mathematical Methods for Physics and Engineering, third ed., Cambridge University Press, 2006.
- [35] S.C. Lowry, P.R. Weissman, S.R. Duddy, B. Rozitis, A. Fitzsimmons, S.F. Green, M.D. Hicks, C. Snodgrass, S.D. Wolters, S.R. Chesley, J. Pittichová, P. van Oers, 5. The internal structure of asteroid (25143) itokawa as revealed by detection of YORP spin-up, Astron. Astrophys. (2014) http://dx.doi.org/10.1051/0004-6361/201322602.
- [36] D.R. Brooks, An introduction to orbit dynamics and its application to satellite-based earth monitoring systems, Tech. Rep., (NASA-TM-X-73605) NASA, 1977, URL https://ntrs.nasa.gov/api/citations/19780004170/downloads/ 19780004170.pdf.

- [37] R. Borase, D. Maghade, Sondkar, A review of PID control, tuning methods and applications, SpringerLink 9 (2020) http://dx.doi.org/10.1007/s40435-020-00665-4.
- [38] K. Wang, Z. Chen, Z. Wei, F. Lu, J. Li, A new smoothing technique for bangbang optimal control problems, in: AIAA Science and Technology Forum and Exposition (SciTech), 2023, http://dx.doi.org/10.2514/6.2024-0727.
- [39] Y. Xie, Y. Lei, J. Guo, B. Meng, Spacecraft attitude control, in: Spacecraft Dynamics and Control, Springer Singapore, Singapore, 2022, pp. 263–370, http://dx.doi.org/10.1007/978-981-33-6448-6-6.
- [40] H. Sawada, R. Okazaki, S. Tachibana, et al., Hayabusa2 sampler: Collection of asteroidal surface material, Space Sci. Rev. 208 (2017) 81–106, http://dx.doi. org/10.1007/s11214-017-0338-8.
- [41] Wikipedia, Bang-bang control, 2024, URL https://en.wikipedia.org/wiki/Bang% E2%80%93bang\_control (Accessed 27 June 2024).
- [42] J. Souchay, C. Lhotka, G. Heron, Y. Hervé, V. Puente, M. Folgueira Lopez, Changes of spin axis and rate of the asteroid (99942) apophis during the 2029 close encounter with earth: A constrained model, Astron. Astrophys. 617 (2018) A74, http://dx.doi.org/10.1051/0004-6361/201832914.
- [43] S. Wagner, D. Zimmerman, B. Wie, Preliminary design of a crewed mission to asteroid apophis in 2029–2036, in: AIAA Guidance, Navigation, and Control Conference, 2010, http://dx.doi.org/10.2514/6.2010-8374.
- [44] K. Berry, P. Antreasian, M.C. Moreau, A. May, B. Sutter, OSIRIS-REx touch-and-go (TAG) navigation performance, in: 38th Annual AAS Guidance and Control Conference, American Astronautical Society, Breckenridge, Colorado, 2015, AAS 15-125.
- [45] S. Kikuchi, T. Saiki, Y. Takei, F. Terui, N. Ogawa, Y. Mimasu, G. Ono, K. Yoshikawa, H. Sawada, H. Takeuchi, H. Ikeda, A. Fujii, S. Sugita, T. Morota, M. Yamada, R. Honda, Y. Yokota, N. Sakatani, S. Kameda, T. Kouyama, N. Hirata, N. Hirata, K. Shirai, K. Kitazato, S. Nakazawa, M. Yoshikawa, S. Tanaka, K. Wada, S. ichiro Watanabe, Y. Tsuda, Hayabusa2 pinpoint touchdown near the artificial crater on ryugu: Trajectory design and guidance performance, Adv. Space Res. 68 (8) (2021) 3093–3140, http://dx.doi.org/10.1016/j.asr.2021.07.031, URL https://www.sciencedirect.com/science/article/pii/S0273117721006037.
- [46] K. Lakshmi, P. Priyadarshi, Multi-disciplinary analysis of a reentry vehicle, in: Advances in Multidisciplinary Analysis and Optimization, Springer, 2020, pp. 19–31, http://dx.doi.org/10.1007/978-981-15-5432-2\_2.
- [47] S. Ershkov, D. Leshchenko, Revisiting apophis 2029 approach to earth (staying on shoulders of nasa's experts) or can we be sure in almost ricocheting fly-by of apophis on 13 of april 2029 near the earth? J. Space Saf. Eng. 9 (3) (2022) 363–374, http://dx.doi.org/10.1016/j.jsse.2022.05.007, URL https://www.sciencedirect.com/science/article/pii/S2468896722000453.
- [48] J.T. Grundmann, W. Bauer, J. Biele, R. Boden, M. Ceriotti, F. Cordero, B. Dachwald, E. Dumont, C.D. Grimm, D. Herčík, T.-M. Ho, R. Jahnke, A.D. Koch, A. Koncz, C. Krause, C. Lange, R. Lichtenheldt, V. Maiwald, T. Mikschl, E. Mikulz, S. Montenegro, I. Pelivan, A. Peloni, D. Quantius, S. Reershemius, T. Renger, J. Riemann, M. Ruffer, K. Sasaki, N. Schmitz, W. Seboldt, P. Seefeldt, P. Spietz, T. Spröwitz, M. Sznajder, S. Tardivel, N. Tóth, E. Wejmo, F. Wolff, C. Ziach, Capabilities of gossamer-1 derived small spacecraft solar sails carrying mascot-derived nanolanders for in-situ surveying of NEAs, Acta Astronaut. 156 (2019) 330–362, http://dx.doi.org/10.1016/j.actaastro.2018.03.019, URL https://www.sciencedirect.com/science/article/pii/S009457651731398X.
- [49] M. Ceriotti, G. Viavattene, I. Moore, A. Peloni, C.R. McInnes, J.T. Grundmann, Sailing at the brink the no-limits of near-/now-term-technology solar sails and SEP spacecraft in (multiple) NEO rendezvous, Adv. Space Res. 67 (9) (2021) 3012–3026, http://dx.doi.org/10.1016/j.asr.2020.10.017, URL https://www.sciencedirect.com/science/article/pii/S0273117720307286. Solar Sailing: Concepts, Technology, and Missions II.
- [50] A. Peloni, B. Dachwald, M. Ceriotti, Multiple near-earth asteroid rendezvous mission: Solar-sailing options, Adv. Space Res. 62 (8) (2018) 2084–2098, http: //dx.doi.org/10.1016/j.asr.2017.10.017, URL https://www.sciencedirect.com/ science/article/pii/S027311771730755X. Past, Present and Future of Small Body Science and Exploration.
- [51] M. Golestani, K.A. Alattas, S.U. Din, F.F.M. El-Sousy, S. Mobayen, A. Fekih, A low-complexity PD-like attitude control for spacecraft with full-state constraints, IEEE Access 10 (2022) 30707–30715, http://dx.doi.org/10.1109/ACCESS.2022. 3159480.